Chemical Science

ROYAL SOCIETY OF CHEMISTRY

EDGE ARTICLE

View Article Online
View Journal | View Issue

Cite this: *Chem. Sci.*, 2022, **13**, 5734

All publication charges for this article have been paid for by the Royal Society of Chemistry

Received 20th February 2022
Accepted 13th April 2022

DOI: 10.1039/d2sc01077a

rsc.li/chemical-science

Angle-dependent strength of a single chemical bond by stereographic force spectroscopy†

Wanhao Cai, [a] Jakob T. Bullerjahn, [b] Max Lallemang, [ac] Klaus Kroy, [d] Bizan N. Balzer *[ace] and Thorsten Hugel *[ac]

A wealth of chemical bonds and polymers have been studied with single-molecule force spectroscopy, usually by applying a force perpendicular to the anchoring surface. However, the direction-dependence of the bond strength lacks fundamental understanding. Here we establish stereographic force spectroscopy to study the single-bond strength for various pulling angles. Surprisingly, we find that the apparent bond strength increases with increasing pulling angle relative to the anchoring surface normal, indicating a sturdy mechanical anisotropy of a chemical bond. This finding can be rationalized by a fixed pathway for the rupture of the bond, resulting in an effective projection of the applied pulling force onto a nearly fixed rupture direction. Our study is fundamental for the molecular understanding of the role of the direction of force application in molecular adhesion and friction. It is also a prerequisite for the nanoscale tailoring of the anisotropic strength of bottom-up designed materials.

Introduction

The reaction of a system to an external force and its direction is one of the most fundamental topics in chemistry and physics. A direction-dependent response to applied forces matters for a wide variety of systems across all scales (Fig. 1). For a bottom-up comprehensive understanding and control of this effect, the mechanics of the smallest load-bearing elements, *i.e.*, single molecular bonds, needs to be characterized. Throughout the last three decades, individual bonds have been extensively studied by atomic force microscopy (AFM)-based single-molecule force spectroscopy (SMFS) using vertical pulling ($\theta = 0°$, Fig. 2).[1–10] However, the direction-dependence of the rupture force of a bond has hardly been systematically studied. For mechanophores the role of topology and force-transduction by polymer chains has already been noted a decade ago,[11,12] but the effect of force vectors on single molecular bonds has remained largely unclear. In addition, coarse-grained theoretical approaches like molecular dynamics (MD) simulations rely on spherical symmetric force fields, and therefore lack abilities to provide molecular details for direction-dependent bond rupture.

In this study, we develop AFM-based stereographic force spectroscopy to investigate the strength of single surface bonds along various pulling directions. Forces are applied at defined, preset pulling angles by simultaneously driving the *z*- and *x*-piezos with nanometer accuracy (Fig. S1†).[13–15]

Note that several potential confounding effects, such as vertical or lateral deflections and torsions of the cantilever, as well as the accuracy of the piezo system, may induce errors in stereographic pulling. We have largely eliminated these effects in our experiments and shown that the remaining uncertainties are negligible. The details of the analysis can be found in the *Analysis of various effects in stereographic pulling* in the ESI and Fig. S2 and S3.†

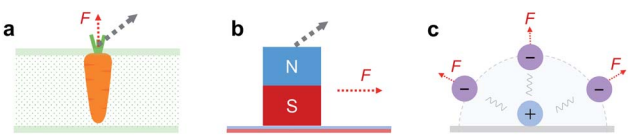

Fig. 1 Different preferential force directions for easiest displacement (red dotted arrows): (a) pulling a carrot out of soil with a preferred vertical direction, (b) pulling a magnet from a magnetic surface with a preferred horizontal direction, (c) separation of point charges without any preferred direction. Here we determine, which model is more appropriate for single chemical bond rupture at a surface. Gray dotted arrows: examples of non-preferential directions, leading to higher rupture or detachment forces.

[a]*Institute of Physical Chemistry, University of Freiburg, Albertstr. 21, 79104, Freiburg, Germany. E-mail: bizan.balzer@pc.uni-freiburg.de; thorsten.hugel@pc.uni-freiburg.de*

[b]*Department of Theoretical Biophysics, Max Planck Institute of Biophysics, Max-von-Laue-Straße 3, 60438, Frankfurt am Main, Germany*

[c]*Cluster of Excellence livMatS@FIT – Freiburg Center for Interactive Materials and Bioinspired Technologies, University of Freiburg, Georges-Köhler-Allee 105, 79110, Freiburg, Germany*

[d]*Institute for Theoretical Physics, Leipzig University, Brüderstraße 16, 04103, Leipzig, Germany*

[e]*Freiburg Materials Research Center (FMF), University of Freiburg, Stefan-Meier-Str. 21, 79104, Freiburg, Germany*

† Electronic supplementary information (ESI) available. See https://doi.org/10.1039/d2sc01077a

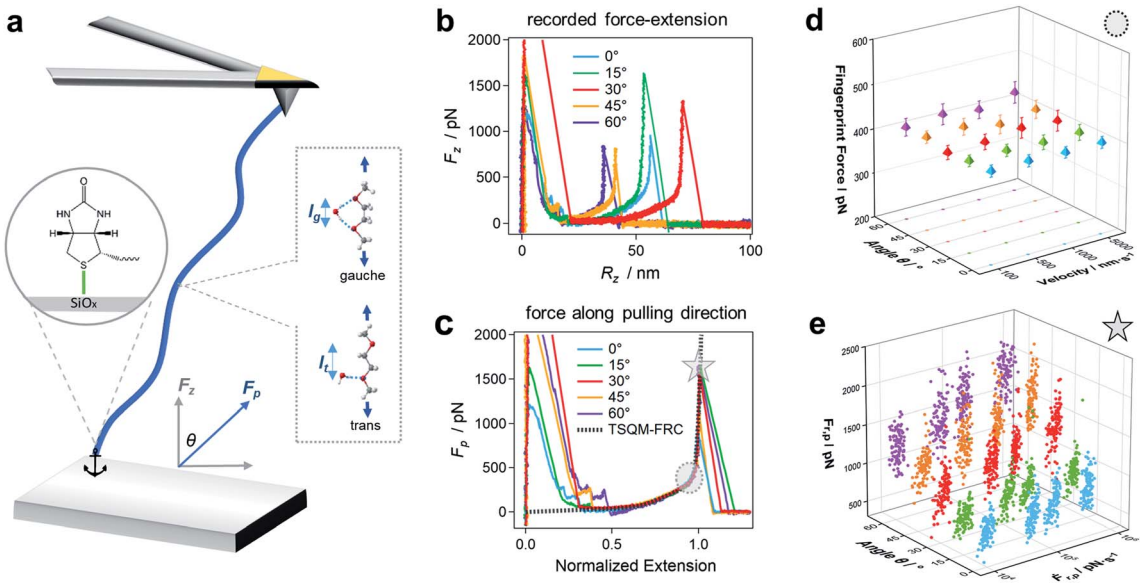

Fig. 2 Angle-dependent elastic response and anchor bond rupture. (a) The angle θ is defined as the angle between the polymer and the normal to the surface, *i.e.*, vertical pulling corresponds to $\theta = 0°$. The PEG monomers switch between gauche/trans states upon stretching in H_2O. (b) Original recorded vertical force F_z *vs.* vertical extension R_z curves of PEG for various angles. (c) After conversion to the force F_p along the pulling direction and the normalized extension, the curves shown in (b) can be superposed. The curves are smoothed with a binomial filter for better presentation. A transition kink can be observed at approximately 400 pN (indicated by a circle), which is the fingerprint of the PEG force–extension curves in H_2O. The force peak in each curve is the rupture force of the anchor bond (indicated by a star). (d) The mean fingerprint force along the pulling direction ($n = 100$ for each case) remains constant for various pulling angles and velocities. (e) The rupture force $F_{r,p}$ along the pulling direction ($n = 100$ for each case) increases with the angle θ and the associated loading rate $\dot{F}_{r,p}$.

Results and discussion

First, we study the chemical bond strength between biotin and a glass surface, with a single polyethylene glycol (PEG) chain acting as a linker. This can result in a sulfur-glass bond as an anchor to the surface in H_2O (Fig. 2a),[16–18] whose strength will be tested in the following experiments under different pulling angles. The formation of such an anchor bond is further validated by three different systems (PEG-thiol, PEG-methoxy, PEG-NHS on glass, respectively, see Fig. S4†): rupture events at high forces (>400 pN) are only observed for PEG-thiol, confirming that these rupture events originate from the sulfur-glass bond and not from any non-specific interactions between the PEG chain and the substrate. Starting from vertical pulling ($\theta = 0°$), we collect several hundred (n >500) force–extension curves, where high stretching forces (F_p >500 pN) can be observed. Such high forces allow us to see the well-defined force–extension fingerprint (kink) of PEG at around 400 pN for vertical pulling (Fig. 2b), which has previously been ascribed to the force-induced gauche–trans transition of PEG monomers in H_2O (Fig. 2a).[19] This well-understood kink is a crucial control for the following stereographic pulling experiments.

Then, we show that the force can be transmitted to the anchor bond along the pulling direction *via* the PEG chain. This is evident from the constant single-chain elasticity of PEG during stereographic pulling at different angles as detailed in the following. The recorded PEG force–extension curves are shown in Fig. 2b. Here, the recorded force F_z is the vertical ($\theta = 0°$) component of the force along the pulling direction F_p (see Fig. 2a), because the AFM cantilever deflects and records the force in the vertical direction. To recover the force–extension curve along the pulling direction, we convert the force F_z to F_p with the corresponding pulling angle θ ($\theta = 0°$ for vertical pulling):

$$F_p = \frac{F_z}{\cos(\theta)} \tag{1}$$

Similarly, we obtain $R_p = R_z \cos(\theta)^{-1}$ for the chain extension along the pulling direction (see *Reconstruction of the curves along pulling direction* in ESI and Fig. S4 for details†). Then, we normalize the traces under different angles as shown in Fig. 2c (see Fig. S5–S7 for details†). These force–extension curves can be well superposed, confirming that the elastic response of a polymer chain does not depend on the pulling direction.

In addition, we can fit the PEG force–extension curves in the whole force region and for different pulling angles with a two-state (gauche, trans) coupled freely rotating chain model, where the elastic stretching modulus γ of PEG at high forces is obtained from quantum mechanical calculations (TSQM-FRC model, see *Single-chain elasticity model* in ESI†):[20]

$$R_N = \left[\frac{l_t}{e^{\frac{-\Delta G + F\Delta L}{k_B T}} + 1} + \frac{l_g}{e^{\frac{\Delta G - F\Delta L}{k_B T}} + 1} \right] \left(\frac{F}{\gamma} + 1 \right) \frac{[1 - (k_B T)/(2Fl_b)]}{l_t} \tag{2}$$

Here, R_N is the normalized extension, l_g, l_t, l_b, ΔL are all fixed structural parameters of PEG, thus leaving the free energy difference (ΔG) between the two states as the only unknown parameter.[19] As shown in Fig. 2c and S5,† the PEG force–extension curves in H_2O can be well fitted with $\Delta G = 3.6\ k_BT$, in good agreement with previous reports in H_2O (3 to 4 k_BT).[19,21]

Fig. 2d shows that the mean fingerprint (kink) position is also independent on the pulling velocity (along the pulling direction) in the range accessible by AFM, indicating that the chain is in a quasi-equilibrium in our study.[22] This is reasonable because of the very fast relaxation of conformational changes on the picosecond timescale:[19,23] the PEG chain reacts faster than the timescale of the experiment to the applied pulling force, and thus always gets rearranged along the pulling direction. This conclusion is also supported by the results of several previous studies on single-chain elasticity using similar or different technical methods.[24–27]

Now we assess the rupture force of the bond at the surface in an angle-dependent way, which has not been done before. Therefore, we determine the rupture force $F_{r,p}$ and loading rate $\dot{F}_{r,p}$ along the pulling direction and construct angle-dependent dynamic force spectra. Fig. 2e shows that $F_{r,p}$ increases with $\dot{F}_{r,p}$ as expected, since the bond rupture is a non-equilibrium process.[28] Surprisingly, $F_{r,p}$ also increases with increasing pulling angle θ: this means that the anchor bond strength seemingly changes with the pulling direction. For a pulling velocity of 5000 nm s^{-1}, the mean $F_{r,p}$ is 949 ($\pm$173) pN for $\theta = 0^\circ$ and almost doubles for $\theta = 60^\circ$, giving 1832 ($\pm$228) pN. Note that a force of approx. 2000 pN is usually associated with the rupture of a covalent bond.[1,29,30] As this force acts on all bonds within the PEG chain, one could expect bond ruptures anywhere between the anchoring points. We have observed hundreds of rupture events at rupture forces higher than 1500 pN ($n = 257$) and find that these high rupture forces and the respective rupture positions remain constant throughout the experiment (Fig. S8†). As the force–extension curves can be repeated obtaining the same signature for hundreds of consecutive curves with the same PEG-biotin functionalized AFM cantilever tip on the same glass substrate, these results validate that the rupture almost always happens at the anchor bond, which is consistent with recent studies on pathogen adhesin.[31] This means that the bonds within the polymer chain are still stronger than the anchor bond even under the imposed conditions of oblique pulling, as required for stereographic force spectroscopy.

To determine the underlying mechanism of the angle-dependence of the bond strength, we construct the free-energy landscape of the bond for different pulling angles and obtain the rupture pathway. This is commonly done by analyzing the rupture forces *via* the Bell–Evans model,[32] which is based on the heuristic Bell rate[33] that is accurate on the force scale of a few pN. At higher forces, the Bell rate only offers a crude approximation, as seen by the fact that the Bell–Evans variance of the rupture force (and all higher moments) deviate strongly from Brownian dynamics simulation data.[28] Instead, we rely on the microscopically exact Dudko–Hummer–Szabo (DHS) model,[28,34] which predicts the following functional form for the force-dependent dissociation rate (see *Rupture force data analysis* in ESI†):

$$k(F) = k_0\left[1 - \frac{F}{F_c}\right]^{\frac{1}{\nu}-1} e^{\frac{\Delta G_u}{k_BT}\left[1-\left(1-\frac{F}{F_c}\right)^{\frac{1}{\nu}}\right]} \quad (3)$$

This expression holds for rupture forces F below the critical force $F_c = \Delta G_u(\nu x_u)^{-1}$, where ΔG_u denotes the height of the free-energy barrier, x_u is the distance from the bound state to the barrier, and ν is a dimensionless parameter that can take the values $\nu = 1/2$, $\nu = 2/3$, and $\nu = 1$. The former two values correspond to cusp and linear-cubic free-energy profiles respectively, while the latter value reduces eqn (3) to the Bell rate.[28] The Bell rate is also retrieved for arbitrary ν-values in the low-force limit $F \ll F_c$. Note that $k(F = 0)$ coincides with the spontaneous escape rate k_0. In order to precisely extract the parameters, we build a systematic protocol to remove the outliers and fit the DHS model with $\nu = 2/3$ to our data *via* the maximum likelihood method (Fig. S9†). Our choice of ν is based on the assumption that the corresponding free energy profile has a smooth barrier, but consistent results are also obtained for $\nu = 1/2$. We provide a fast open-source implementation of our data fitting protocol for the analysis of rupture force spectra.[35]

The rupture of a bond is tentatively ascribed to either of two idealized rupture scenarios, which we call the aligned-pathway and fixed-pathway scenario, respectively (Fig. 3a and b). In the *aligned-pathway scenario*, the bond is assumed to rupture along the direction of the pulling force.[36,37] This describes a flexible bond angle as it implies that the system can easily be bent and rotated by force, such that the rupture direction follows the pulling direction. This would correspond to Fig. 1c that describes no preferred rupture direction of a bond. As shown in Fig. 3c, the force spectra can be fitted with this model for each angle separately. However, for this aligned-pathway scenario, different parameters are obtained for different pulling angles. As the bond is the same, these parameters should actually be similar for each pulling angle.

Therefore we now test the *fixed-pathway scenario*, where the bond direction is strongly confined by its geometry, *i.e.*, where the bond angle is largely fixed and stays nearly constant upon pulling.[38,39] That is, rather than adjusting to the bond direction, the bond ruptures along the same single pathway for all pulling angles. This would correspond to Fig. 1a that describes a highly preferred rupture direction of a bond. In this fixed-pathway scenario, in which the force and bond directions are generally misaligned, only the force projection along the pathway contributes to bond rupture.[40] Taking $\theta = 0^\circ$ as the ideal pathway direction of the surface bond, as commonly assumed in vertical pulling assays, a global fit is applied to the vertical component of rupture force and loading rate ($\dot{F}_{r,z}$ *vs.* $\dot{F}_{r,z}$) for all angles. Surprisingly, the results for the $\theta = 0^\circ$ fit and the global fit are in very good agreement (Fig. 3d), validating that the bond ruptures along the same pathway for all angles. As only the

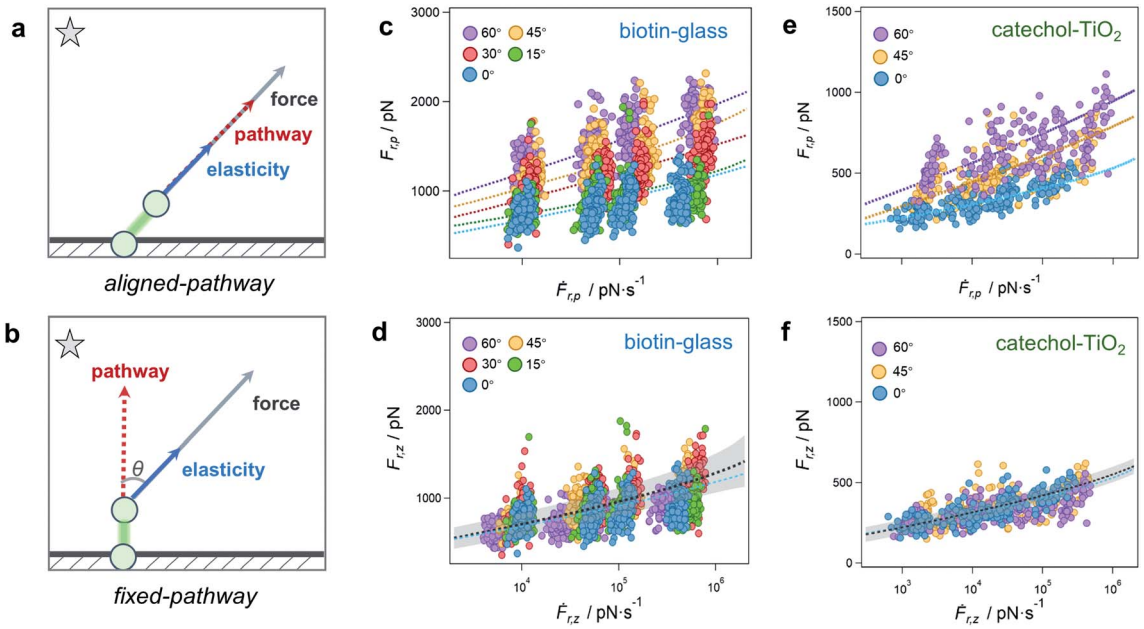

Fig. 3 Angle-dependent anchor bond strength. Diagram of the aligned-pathway (a) and the fixed-pathway scenario (b), respectively. For each scenario, the mean rupture force (MRF) predictions of the DHS model (dotted lines) evaluated using fit parameters obtained from maximum likelihood estimation for fixed $v = 2/3$, are compared to measured rupture forces (filled dots). (c) Forces and loading rates along the pulling direction ($F_{r,p}$ *vs.* $\dot{F}_{r,p}$) of a biotin-glass bond in the aligned-pathway scenario. Notably, the MRFs for different pulling directions do not overlap. (d) Projecting forces and loading rates of the biotin-glass bond along vertical direction ($F_{r,z}$ *vs.* $\dot{F}_{r,z}$), as suggested by the fixed-pathway scenario, the rupture forces measured at different pulling angles nicely overlap with consistent MRFs. Shown are the MRFs evaluated using the global fit values (black dotted line), and the optimal parameters for the $\theta = 0°$ data (blue dotted line). To visualize the underlying distribution of rupture forces, we indicate the standard deviation above and below the MRF of the global fit by a grey-shaded area. (e and f) Rupture forces and loading rates of a catechol–TiO_2 bond in the aligned- and fixed-pathway scenarios analysed in the same way as the biotin-glass bond, with similar results.

vertical force component affects the bond rupture under angle-dependent pulling, higher apparent rupture forces $F_{r,p}$ along the pulling direction are required for steeper angles to provide enough force in vertical direction.

To further validate the direction-dependence of chemical bonds, the catechol–TiO_2 bond is studied as a second system ($n = 200$ for each angle, Fig. 3e and f).[41,42] We note that catechol can be easily oxidized to quinone under high pH and hence leads to different bond types and rupture forces with TiO_2.[43] To ensure the formation of the catechol–TiO_2 bond, the experiments are carried out under pH 3, where catechol remains unoxidized. Similar to the biotin-glass experiments, the force is transmitted to the catechol–TiO_2 bond along the pulling direction *via* a PEG chain (Fig. S10†). We again observe an increase of $F_{r,p}$ for larger angles, while $F_{r,z}$ stays nearly constant. This indicates that the force direction plays a universally important role for the perceived strength of single chemical bonds at surfaces, which are much less flexible than one might have thought.

The fit results indicate a barrier height ΔG_u of 14 to 17 k_BT for both the biotin-glass bond and the catechol–TiO_2 bond (see Tables S1–S4 for fit parameters†), comparable to a coordination/covalent bond.[30,44] Such an anchor strength prevents the target molecule from slipping on the surface,[14] which is essential to obtain a well-defined angle when driving the piezo positioning system in vertical and lateral directions, respectively.

Conclusions and outlook

We use stereographic force spectroscopy to study how the direction of an applied force affects the strength of single chemical bonds at a surface. We find that the apparent bond strength increases with increasing pulling angle. Dynamic stereographic force spectroscopy then allows us to determine the bond rupture pathway. Surprisingly, we find that an anchor bond ruptures along a fixed pathway, resulting in an effective projection of the applied pulling force onto a nearly fixed rupture direction.

The direction-dependence of the surface bond strength constitutes a sturdy mechanical anisotropy, in particular when the distinction between adhesion ($\theta = 0°$) and friction ($\theta = 90°$) properties matters (as in the extreme scenarios of Fig. 1a and b). As an example, it could be exploited to adjust the adhesion strength of cells or other objects on surfaces. Stiff directional bonds would allow cells to withstand higher shear forces (*e.g.*, due to blood flow), while flexible bonds would facilitate their sliding. Such principles could also guide the bottom-up design of chemical materials, coatings and lubricants. Low friction could be designed by engineering interfacial bonds or interactions that can quickly adapt to the direction of force application (scenario of Fig. 1c) or that show a high in-plane mobility (scenario of Fig. 1b), which has been observed in graphene systems with interfacial π–π stacking.[45] High friction is

expected for directional bonds (scenario of Fig. 1a), as shown here for a stiff chemical bond. Even friction-switchable interfaces can be thought of, where the stiffness and therefore the direction-dependence of bonds can be switched by an external stimulus, such as for azobenzene. Finally, we anticipate that the inclusion of direction-dependence will contribute to advanced force fields for MD simulations, which currently only have a spherical symmetry (scenario of Fig. 1c). Altogether, our results quantify and highlight the importance of directionality of force application for the anchoring of polymers to surfaces and potentially for any interface.

Materials and methods

Materials and sample preparation

All the chemicals are analytically pure and used without further treatment, if not mentioned otherwise. Triethoxysilane-PEG-biotin and triethoxysilane-PEG-methoxy are purchased from Rapp Polymere (Tübingen, Germany, M_w = 5 kDa), triethoxysilane-PEG-thiol (M_w = 5 kDa) and triethoxysilane-PEG-NHS (M_w = 5 kDa) are purchased from NANOCS (Boston, MA, USA). Dopamine hydrochloride is purchased from Sigma-Aldrich (St. Louis, MO, USA). Glass substrate (Borosilicate glass from hydrolytic class I) is purchased from Carl Roth (Germany). TiO_2 substrate is prepared as reported in the literature.[46]

The glass substrates are cleaned as follows: firstly, they are cleaned ultrasonically for 10 min with H_2O and methanol and respectively. Secondly, they are immersed in RCA solution at 60 °C for 1 hour. RCA comprises a volume ratio of 5 : 1 : 1 of H_2O (Purelab Chorus 1, Elga LabWater, Celle, Germany, 18.2 MΩ cm), NH_3 solution (Roth, Karlsruhe, Germany, 28.0–30.0%), H_2O_2 (Sigma-Aldrich, St. Louis, MO, USA, ≥30%). Then, they are rinsed with extensive H_2O to remove the residual RCA solution. The TiO_2 substrates are cleaned ultrasonically for 10 min with H_2O and methanol respectively, then activated with oxygen plasma (40% power, 0.1 mbar, 2 min, Diener Electronics, Germany). The tweezers and glassware are cleaned as follows: firstly, they are immersed in RCA solution at 60 °C for 1 hour, followed by rinsing with extensive H_2O; then, they are dried and stored at 120 °C.

AFM cantilever tip functionalization

Si_3N_4 AFM cantilevers (MLCT-BIO-DC, Bruker AFM probes, Camarillo, CA, USA) are used in the force measurements. The cantilevers are activated with oxygen plasma (40% power, 0.1 mbar, 2 min, Diener Electronics, Germany) to generate hydroxyl groups on the cantilever surface.

Then, for the functionalization with biotin, the cantilevers are incubated in a solution of triethoxysilane-PEG-biotin in toluene (1.25 mg mL^{-1}, 2 h, 22 °C), then rinsed with toluene, ethanol and H_2O respectively to get rid of the loosely adsorbed molecules. For the functionalization with catechol, the cantilevers are incubated in a solution of triethoxysilane-PEG-NHS in toluene (1.25 mg mL^{-1}, 2 h, 22 °C), then rinsed with toluene, ethanol and H_2O respectively. After that, these cantilevers are further incubated in a solution of dopamine in PBS buffer (pH = 7.2, 1 h, 22 °C), rinsed 3 times with PBS buffer. For the functionalization with thiol, NHS and methoxy groups, the AFM cantilevers are incubated in a solution of triethoxysilane-PEG-thiol, triethoxysilane-PEG-NHS and triethoxysilane-PEG-methoxy in toluene (1.25 mg mL^{-1}, 2 h, 22 °C), then rinsed with toluene, ethanol and H_2O, respectively. Finally, all cantilevers are stored in H_2O and used in experiments within 3 days.

AFM-based single-molecule force spectroscopy

All vertical pulling ($\theta = 0°$) SMFS experiments are performed with a MFP3D-Bio (Asylum Research, an Oxford Instruments company, CA, USA) using a fluid cell at room temperature (22 °C). The biotin-glass and thiol-glass experiments are carried out in H_2O, while the catechol–TiO_2 experiments are carried out in ROTI Calipure buffer solution (pH 3.0, Roth, Karlsruhe, Germany).[43] Before the experiment, the inverse optical lever sensitivity (InvOLS) is determined by a linear function to the repulsive regime of a force–extension curve and using an average of at least five InvOLS values. The spring constant of the cantilever is determined by the thermal noise method. The details of the AFM instrumentation can be found elsewhere.[47,48]

AFM-based stereographic force spectroscopy

All stereographic force spectroscopy experiments are performed with the same MFP3D-Bio. A self-written program based on the functions of Asylum Research and Igor Pro, is used to control the movement of the cantilever tip and the scanner (surface). The pulling angle and velocity are realized by driving the *z*- and *x*-piezos simultaneously with respective defined velocities, hence applying a stereographic force on the bond. Herein, the *x*-piezo is defined as the piezo that drives the surface perpendicular to the cantilever axis. The stereographic pulling can be divided into 4 stages: (1) a cantilever tip functionalized with the target molecule is approached to the surface vertically. (2) The cantilever tip contacts the surface with a certain force trigger (approx. 2–10 nN, contact time approx. 0.01–2 s), leading to a contact between cantilever tip and the surface underneath. During the respective contact, the target molecule binds to the surface, *i.e.*, the molecule is anchored. (3) The cantilever tip is retracted with a distance corresponding to the indentation depth. (4) The cantilever tip is further retracted vertically while the piezo system moves the cantilever laterally, which allows the pulling of the target molecule with different angles and velocities. There, the PEG-substrate interaction and solvent related (hydrodynamic) friction of PEG in solution is below the detection limit of our experiment.[49]

During the measurement, the vertical deflection of the cantilever and the ZLVDT (*z*-piezo movement) are recorded for generating the vertical force–extension curves. The YLVDT, XLVDT, and lateral deflections of the cantilever, are also recorded for further evaluation.

Analytical protocol of dynamic force spectra

The Dudko–Hummer–Szabo (DHS) model is used to analyze the measured rupture forces and the associated loading rates using

the maximum likelihood method, and hence to extract the kinetics of the anchor bond under different pulling angles. To perform a reliable analysis, we have built a systematic protocol to optimize the fit quality, which considers the evolution of the fit parameters while trimming rupture force data. A detailed description can be found in the *Rupture force data analysis* in ESI.†

Data availability

The data supporting the findings of this study are available within the article and in the ESI.† The raw data are available from the authors upon reasonable request.

Author contributions

W. C., B. N. B. and T. H. designed the study, W. C. and M. L. performed experiments, J. T. B. and W. C. performed the fitting process of bond rupture and elasticity models, W. C. and J. T. B. analyzed data after consultation with K. K., B. N. B. and T. H., W. C., B. N. B. and T. H. wrote the manuscript, J. T. B and K. K. revised the manuscript. All authors discussed the results and commented on the manuscript.

Conflicts of interest

There are no conflicts to declare.

Acknowledgements

This work is supported by the Deutsche Forschungsgemeinschaft (DFG, German Research Foundation) under Germany's Excellence Strategy – EXC-2193/1 – 390951807 (ML, TH and BNB) and the grant HU 997/13-1 (WC and TH). The authors thank Roland Netz (FU Berlin) and Steffen Wolf (University of Freiburg) for helpful discussions, Gerhard Hummer (MPI of Biophysics, Frankfurt) for helpful feedback on the manuscript and Klaus Rischka (Fraunhofer IFAM) for providing samples, JTB acknowledges support by the Max Planck Society.

Notes and references

1 M. Grandbois, M. Beyer, M. Rief, H. Clausen-Schaumann and H. E. Gaub, *Science*, 1999, **283**, 1727–1730.
2 M. Rief, F. Oesterhelt, B. Heymann and H. E. Gaub, *Science*, 1997, **275**, 1295–1297.
3 H. Li, W. A. Linke, A. F. Oberhauser, M. Carrion-Vazquez, J. G. Kerkviliet, H. Lu, P. E. Marszalek and J. M. Fernandez, *Nature*, 2002, **418**, 998–1002.
4 D. T. Edwards, J. K. Faulk, A. W. Sanders, M. S. Bull, R. Walder, M.-A. LeBlanc, M. C. Sousa and T. T. Perkins, *Nano Lett.*, 2015, **15**, 7091–7098.
5 H. Wang and H. Li, *Chem. Sci.*, 2020, **11**, 12512–12521.
6 A. Kolberg, C. Wenzel, K. Hackenstrass, R. Schwarzl, C. Rüttiger, T. Hugel, M. Gallei, R. R. Netz and B. N. Balzer, *J. Am. Chem. Soc.*, 2019, **141**, 11603–11613.
7 W. Cai, D. Xu, L. Qian, J. Wei, C. Xiao, L. Qian, Z.-Y. Lu and S. Cui, *J. Am. Chem. Soc.*, 2019, **141**, 9500–9503.
8 M. J. Jacobs and K. Blank, *Chem. Sci.*, 2014, **5**, 1680–1697.
9 Y. Xue, X. Li, H. Li and W. Zhang, *Nat. Commun.*, 2014, **5**, 4348.
10 C. L. Brown and S. L. Craig, *Chem. Sci.*, 2015, **6**, 2158–2165.
11 H. M. Klukovich, T. B. Kouznetsova, Z. S. Kean, J. M. Lenhardt and S. L. Craig, *Nat. Chem.*, 2013, **5**, 110–114.
12 J. Ribas-Arino and D. Marx, *Chem. Rev.*, 2012, **112**, 5412–5487.
13 F. Kühner, M. Erdmann, L. Sonnenberg, A. Serr, J. Morfill and H. E. Gaub, *Langmuir*, 2006, **22**, 11180–11186.
14 B. N. Balzer, M. Gallei, M. V. Hauf, M. Stallhofer, L. Wiegleb, A. Holleitner, M. Rehahn and T. Hugel, *Angew. Chem., Int. Ed.*, 2013, **52**, 6541–6544.
15 L. Grebíková, S. G. Whittington and J. G. Vancso, *J. Am. Chem. Soc.*, 2018, **140**, 6408–6415.
16 C. R. Peiris, S. Ciampi, E. M. Dief, J. Zhang, P. J. Canfield, A. P. Le Brun, D. S. Kosov, J. R. Reimers and N. Darwish, *Chem. Sci.*, 2020, **11**, 5246–5256.
17 M. Hu, F. Liu and J. M. Buriak, *ACS Appl. Mater. Interfaces*, 2016, **8**, 11091–11099.
18 J. L. Lou, H. W. Shiu, L. Y. Chang, C. P. Wu, Y.-L. Soo and C.-H. Chen, *Langmuir*, 2011, **27**, 3436–3441.
19 S. Liese, M. Gensler, S. Krysiak, R. Schwarzl, A. Achazi, B. Paulus, T. Hugel, J. r. P. Rabe and R. R. Netz, *ACS Nano*, 2017, **11**, 702–712.
20 W. Cai, S. Lu, J. Wei and S. Cui, *Macromolecules*, 2019, **52**, 7324–7330.
21 F. Oesterhelt, M. Rief and H. E. Gaub, *New J. Phys.*, 1999, **1**, 6.1–6.11.
22 D. B. Staple, M. Geisler, T. Hugel, L. Kreplak and H. J. Kreuzer, *New J. Phys.*, 2011, **13**, 013025.
23 B. Heymann and H. Grubmüller, *Chem. Phys. Lett.*, 1999, **307**, 425–432.
24 C. Ke, Y. Jiang, M. Rivera, R. L. Clark and P. E. Marszalek, *Biophys. J.*, 2007, **92**, L76–L78.
25 M. Dendzik, A. Kulik, F. Benedetti, P. E. Marszalek and G. Dietler, *Nanotechnology*, 2013, **24**, 365703.
26 F. Kühner, M. Erdmann and H. E. Gaub, *Phys. Rev. Lett.*, 2006, **97**, 218301.
27 R. Walder, W. J. Van Patten, A. Adhikari and T. T. Perkins, *ACS Nano*, 2018, **12**, 198–207.
28 O. K. Dudko, G. Hummer and A. Szabo, *Phys. Rev. Lett.*, 2006, **96**, 108101.
29 S. W. Schmidt, M. K. Beyer and H. Clausen-Schaumann, *J. Am. Chem. Soc.*, 2008, **130**, 3664–3668.
30 P. Schwaderer, E. Funk, F. Achenbach, J. Weis, C. Bräuchle and J. Michaelis, *Langmuir*, 2008, **24**, 1343–1349.
31 L. F. Milles, K. Schulten, H. E. Gaub and R. C. Bernardi, *Science*, 2018, **359**, 1527–1533.
32 E. Evans and K. Ritchie, *Biophys. J.*, 1997, **72**, 1541–1555.
33 G. I. Bell, *Science*, 1978, **200**, 618–627.
34 S. Getfert and P. Reimann, *Phys. Rev. E: Stat., Nonlinear, Soft Matter Phys.*, 2007, **76**, 052901.
35 See **https://github.com/bio-phys/ForceSpectroscopyMLE** for a Julia implementation of our results.

36 M. Bertz, A. Kunfermann and M. Rief, *Angew. Chem., Int. Ed.*, 2008, **47**, 8192–8195.
37 R. B. Best, E. Paci, G. Hummer and O. K. Dudko, *J. Phys. Chem. B*, 2008, **112**, 5968–5976.
38 T. Hugel, M. Rief, M. Seitz, H. E. Gaub and R. R. Netz, *Phys. Rev. Lett.*, 2005, **94**, 048301.
39 C. Schoeler, R. C. Bernardi, K. H. Malinowska, E. Durner, W. Ott, E. A. Bayer, K. Schulten, M. A. Nash and H. E. Gaub, *Nano Lett.*, 2015, **15**, 7370–7376.
40 E. Evans, *Annu. Rev. Biophys. Biomol. Struct.*, 2001, **30**, 105–128.
41 Y. Li and Y. Cao, *Nanoscale Adv.*, 2019, **1**, 4246–4257.
42 H. Lee, N. F. Scherer and P. B. Messersmith, *Proc. Natl. Acad. Sci. U. S. A.*, 2006, **103**, 12999–13003.
43 S. Krysiak, Q. Wei, K. Rischka, A. Hartwig, R. Haag and T. Hugel, *Beilstein J. Org. Chem.*, 2015, **11**, 828–836.
44 P. Das and M. Reches, *Nanoscale*, 2016, **8**, 15309–15316.
45 O. Hod, E. Meyer, Q. Zheng and M. Urbakh, *Nature*, 2018, **563**, 485–492.
46 M. Lallemang, L. Yu, W. Cai, K. Rischka, A. Hartwig, R. Haag, T. Hugel and B. N. Balzer, *Nanoscale*, 2022, **14**, 3768–3776.
47 A. Kolberg, C. Wenzel, T. Hugel, M. Gallei and B. N. Balzer, *J. Visualized Exp.*, 2020, e60934.
48 Y. Bao, Z. Luo and S. Cui, *Chem. Soc. Rev.*, 2020, **49**, 2799–2827.
49 F. Rico, L. Gonzalez, I. Casuso, M. Puig-Vidal and S. Scheuring, *Science*, 2013, **342**, 741–743.